Direct and precise measurement of displacement and velocity of flexible web in roll-to-roll manufacturing systems

Dongwoo Kang, Young duk Kim, Eonseok Lee, Young-Man Choi, Taik-Min Lee, and Dongmin Kim

Citation: Review of Scientific Instruments **84**, 125005 (2013); doi: 10.1063/1.4831816
View online: http://dx.doi.org/10.1063/1.4831816
View Table of Contents: http://scitation.aip.org/content/aip/journal/rsi/84/12?ver=pdfcov
Published by the AIP Publishing

Direct and precise measurement of displacement and velocity of flexible web in roll-to-roll manufacturing systems

Dongwoo Kang,[1] Young duk Kim,[2] Eonseok Lee,[1] Young-Man Choi,[1] Taik-Min Lee,[1] and Dongmin Kim[3,a)]

[1]*Advanced Manufacturing Systems Research Division, Korea Institute of Machinery and Materials, 156 Gajeongbuk-Ro, Yuseong-Gu, Daejeon 305-343, South Korea*

[2]*Nano-Opto-Mechatronics Lab., Dept. of Mechanical Eng., KAIST, 335 Gwahangno, Yuseong-Gu, Daejeon 305-701, South Korea*

[3]*Korea Research Institute of Standards and Science, 267 Gajeong-Ro, Yuseong-Gu, Daejeon 305-340, South Korea*

(Received 16 September 2013; accepted 3 November 2013; published online 11 December 2013)

Interest in the production of printed electronics using a roll-to-roll system has gradually increased due to its low mass-production costs and compatibility with flexible substrate. To improve the accuracy of roll-to-roll manufacturing systems, the movement of the web needs to be measured precisely in advance. In this paper, a novel measurement method is developed to measure the displacement and velocity of the web precisely and directly. The proposed algorithm is based on the traditional single field encoder principle, and the scale grating has been replaced with a printed grating on the web. Because a printed grating cannot be as accurate as a scale grating in a traditional encoder, there will inevitably be variations in pitch and line-width, and the motion of the web should be measured even though there are variations in pitch and line-width in the printed grating patterns. For this reason, the developed algorithm includes a precise method of estimating the variations in pitch. In addtion, a method of correcting the Lissajous curve is presented for precision phase interpolation to improve measurement accuracy by correcting Lissajous circle to unit circle. The performance of the developed method is evaluated by simulation and experiment. In the experiment, the displacement error was less than 2.5 μm and the velocity error of 1σ was about 0.25%, while the grating scale moved 30 mm.
 [http://dx.doi.org/10.1063/1.4831816]

I. INTRODUCTION

Recently, interest in roll-to-roll manufacturing technology for inexpensive micro electronic devices has gradually increased due to its low mass-production costs and compatibility with flexible substrate. In addition, when cost-effective patterning processes – such as a printing process which can replace the photo-lithographic process[1] for micron-size patterns – are incorporated into a roll-to-roll manufacturing system, it can generate an additional cost benefit. For this reason, many researches are being conducted with a view to creating a new market for roll-to-roll printed electronics.[2–4] Jung *et al.* developed an all-printed and roll-to-roll printable 1-bit Radio frequency identification (RFID) tag on plastic foil,[2] while Krebs fabricated an all-solution roll-to-roll processed polymer solar cell with a power conversion efficiency of 0.3%.[3] Furthemore, RFID tags and several inexpensive functional displays have been demonstrated by several research groups.[4] In the abovementioned researches, one of the major obstacles to improving electronic performance are the patterning resolution and overlay accuracy of roll-to-roll printing systems.[2,4] For example, the drive current density of printed thin-film transistors (TFT) are increased in shorter channel length of TFT, however there is limitation to reduce the channel length due to patterning resolution and overlay precision of roll-to-roll printing system. The inaccuracy of roll-to-roll printing systems originates from combined error sources such as variations in velocity and tension in the web, variations in lateral motion of the web, synchronization errors between the web and the printing master plate, patterning errors in the printing master, and so on. Although several control algorithms have been developed to reduce each error component,[5–8] it is still not sufficiently precise for use in the manufacturing of reliable roll-to-roll printed electronics. One of the major reasons for this is the lack of a solution for measuring the motion of the web precisely, because most of above error sources are related to the precision motion control of the web. General precision measurement systems which is applied in sheet-type manufacturing processes, such as the manufacturing of semiconductors and liquid crystal displays, can't be used in roll-to-roll systems. In those systems, the precision XY stage system is used and the motion of the substrate can be measured precisely by measuring the stage position instead of the substrate itself, because the substrate is rigidly attached to the stage using a vacuum chuck. However, it is not easy to apply a similar approach to the roll-to-roll manufacturing process because there is no area to which the web is rigidly attached, and because the motion of the web should be measured directly on the web. Although there have been some researches in which the motion of the web is measured indirectly by measuring the angular position and radius of the idle roller by assuming that no slip occurs at the contact interface between the web and the roller surface,[9] its accuracy is limited by variations of

a)Author to whom correspondence should be addressed. Electronic mail: dm96.kim@kriss.re.kr. Tel.: +82-42-868-5457.

radius in the rotation bearing system and micro-slip at the contact interface. Several methods of direct measurement of the motion of the web have been tried. Tullis proposed an image-based measurement method in which two image sensors, located some distance apart, are used to capture the same target patterns on the web, with the second sensor taking the image at a predetermined time after the capture time of the first image sensor.[10] This predetermined time can be calculated based on the distance between the two image sensors and the nominal moving speed of the web. After image processing of the two images, the displacement of the web during the predetermined time can be calculated. The accuracy of this method is limited by the calibration accuracy of the distance between the sensors, the image sensor pixel resolution, and the capture rate of the image sensors. Another approach consists in applying a linear encoder to measure the web position by replacing the precision grating scale with printed grating patterns on the web.[11] The accuracy of this method depends on the quality of the printed grating patterns. Actually, because there are necessarily variations of pitch in printed patterns, the accuracy cannot be good enough to measure the motion of the web simply by applying a linear encoder.

For this paper, Oh's measurement method[11] was improved in order to measure the motion of the web precisely, even though there are variations of pitch in printed grating patterns. A novel algorithm to estimate the pitch variation is proposed herein, and the system has been modified to carry out the developed algorithm. The developed algorithm includes a method of generating the sinusoidal encoder signal according to the estimated variation in pitch of the printed grating patterns and the method of correcting the Lissajous curve based on Heydermann method of improving accuracy.[12] The performance of the developed method is evaluated by simulation and experiment. In this paper, proving the concept of the proposed algorithm is focused on and the issues related to real-time signal pocessing and compactness of system are out of scope.

II. NOVEL MEASUREMENT PRINCIPLE FOR MOTION OF THE WEB

A. Traditional single field encoder

The principle of the traditional single field encoder is shown in Fig. 1.[13] Collimated light is projected to scale through the scanning reticle. When a slightly different grating pitch is used in scale from the scanning reticle, the transmitted light forms a moiré image, as shown in Fig. 1(b), which is exposed on the photo detector. The generated moiré image shows two dominant peaks in the spatial frequency spectrum, and the lower envelop frequency, which is given in Eq. (1) when the grating pitch of the scanning reticle is smaller than that of the scale, is used to generate phase-shifted sinusoidal encoder signals,

$$f_b = f_r - f_s, \tag{1}$$

where f_r is the spatial frequency of the reticle grating, f_s is the spatial frequency of the scale grating, and f_b is the envelop frequency in the moiré image. When the photo-sensors are structured so that the size of each pixel becomes a quarter of the period of the lower envelop frequency component, as shown in Fig. 1(b), four 90° phase-shifted sinusoidal signals are gathered at four succesive photo sensors by the movement of the scale relative to the scanning reticle and the photo-sensors at constant speed. In other words, as the scale moves relative to the reticle and the photo-sensors at constant speed, each signal in the photo-sensors undergoes a sinusoidal variation in which one cycle of sine curve is completed with the web movement of single pitch of the scale grating, and the signals in the two adjacent photo sensors show a phase shift of 90°, as shown in Fig. 2. Several sets of the phase-shifted signals ($I_{0,i}$, $I_{90,i}$, $I_{180,i}$, $I_{270,i}$, i = number of sets) are gathered to prevent measurement failure due to scale contamination. The gathered signals are averaged for each phase, and four signals, i.e., I_0, I_{90}, I_{180}, and I_{270} are used to determine the displacement of the scale. Finally, the Lissajous curve is generated by two signals of I_1, I_2 to reduce the shift of origin in the Lissajous curve by removing the DC offset in the signals as follows:

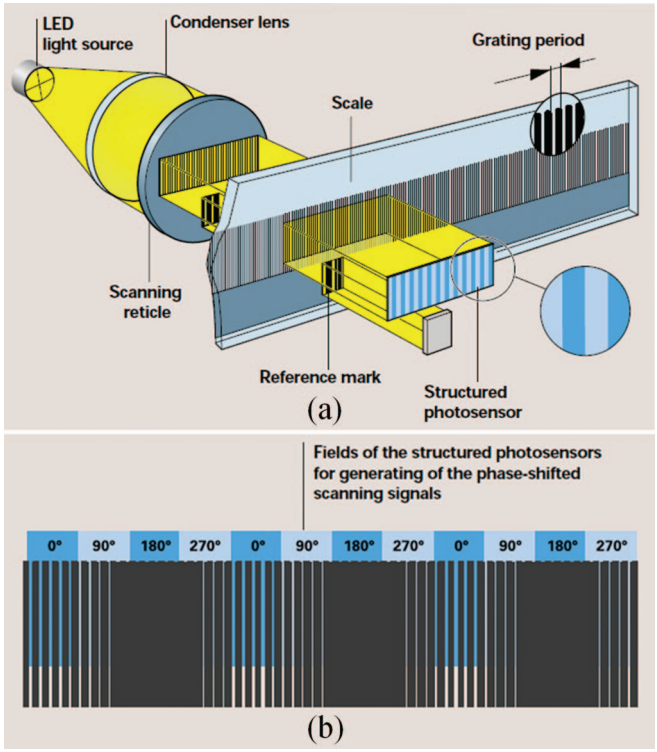

FIG. 1. Principle of traditional single field encoder (www.heidenhain.com):[13] (a) system configuration; (b) transmitted moire pattern on detector plane.

$$I_1 = I_0 - I_{180}, \tag{2}$$

$$I_2 = I_{90} - I_{270}. \tag{3}$$

The resolution of the encoder can be improved by interpolating the phase in the Lissajous curve if the Lissajous curve forms nearly a unit circle. The displacement of the scale can be calculated by the following equation:

$$x = P_s \times (\theta/2\pi). \tag{4}$$

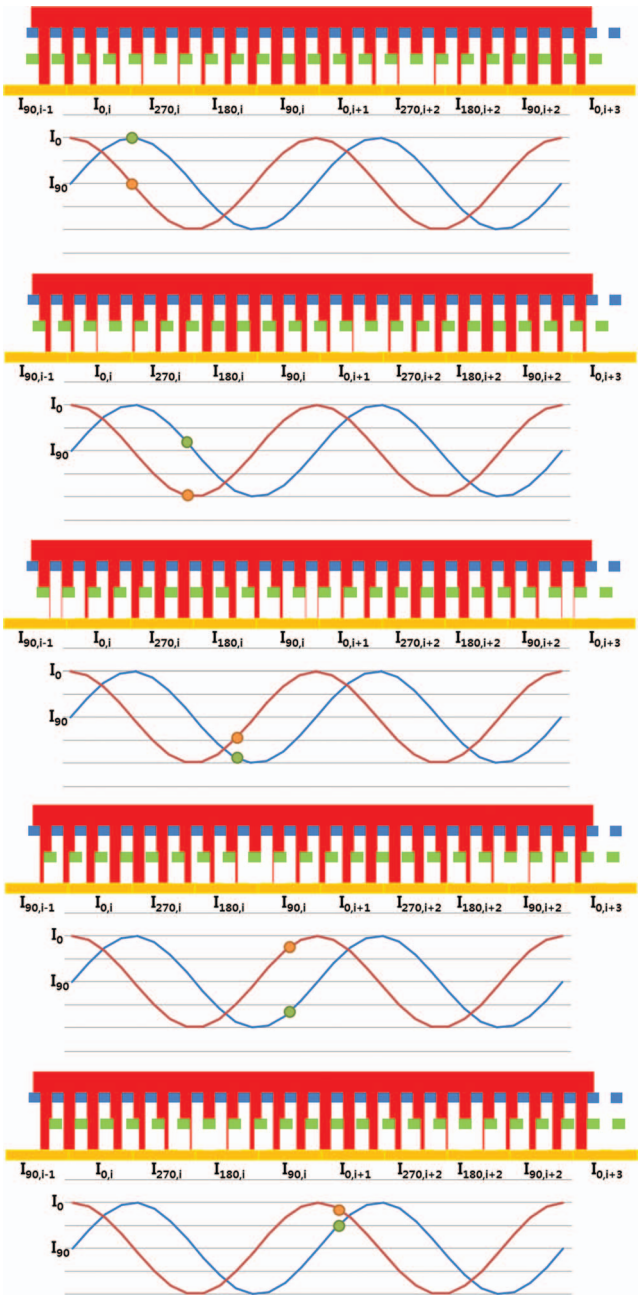

FIG. 2. Measured signal variation with time at each single photo detector. While the web moves a pitch of the scale grating, the envelop of the moiré image moves its pitch.

where x is the displacement of the scale, P_s is the pitch of scale grating, and θ is the delta phase between two successive time stamps. Because there is 2π phase ambiguity in Eq. (2), the maximum measurement velocity limitation occurs

$$V_{\max} = (P_s/2) \times F_s, \tag{5}$$

where $V_{\max}$ is the maximum measurement velocity and F_s is the sampling frequency of the photo sensor.

B. Developed printed grating scale encoder

The displacement of the scale is dependent on the pitch of the grating patterns on the scale as expressed in Eq. (4).

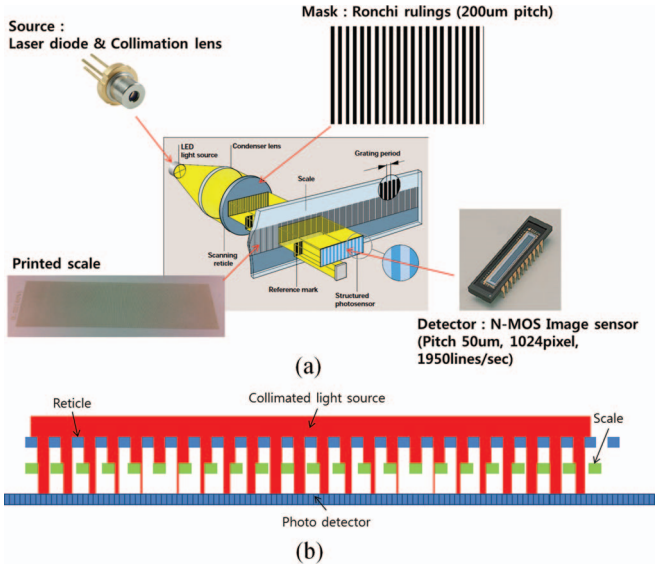

FIG. 3. System configuration of the printed grating scale encoder: (a) system concept; (b) diagram.

This means that the measurement accuracy of the encoder deteriorates when there are variations in the pitch of the grating. In addition, variations in line-width can cause phase interpolation errors due to distortion of the Lissajous circle. In this section, a novel algorithm to measure the motion of the printed web scale precisely is proposed. Because the printed web scale necessarily exhibits variations in pitch and line-width, the algorithm includes a pitch estimation step. In addition, a Lissajous curve correction step is presented for precision phase interpolation to improve measurement accuracy by correcting Lissajous circle to unit circle. Prior to explaining the details of the algorithm, a system configuration of the printed grating scale encoder is introduced in Fig. 3. The collimated beam is generated by a diode laser (#31-2772-000, Coherent Inc.) and a condenser lens and projected on the reticle (Ronchi Rullings, 5.0 c/mm, Applied Images Inc.) like in a traditional encoder. In the proposed setup, a screen-printed grating with pitches slightly larger than those of the scanning reticle is used as the scale grating, and the structured photo sensor is replaced by a NMOS image sensor (S3901-1024Q, Hamamatsu Photonics K. K.), which has 1024 pixels with a pixel size of 50 μm and a line rate of 1950 lines/s. The NMOS image sensor plays an important role in the pitch estimation algorithm. Because the printed scale grating has variations in pitch, the envelop frequency of the moiré image will be varied by Eq. (2). This means that the pitch of the structured photo sensors cannot be fixed and thus should be changed adaptively according to the variations in pitch of the printed scale grating. Slight variation of pitches in the printed scale grating cause a enlarged variation of pitches in the envelop of the moiré image. Actually, the pitch of the envelop frequency varies from 1.533 mm to 4.2 mm according to the pitch variation range of the scale grating, i.e., from 0.21 mm to 0.23 mm. Figure 4(a) shows the moiré image with pitches of 0.21 mm and 0.22 mm, while Fig. 4(b) shows the moiré pattern with pitches of 0.21 mm and 0.23 mm. To divide each sinusoidal phase region precisely, a smaller pixel size is

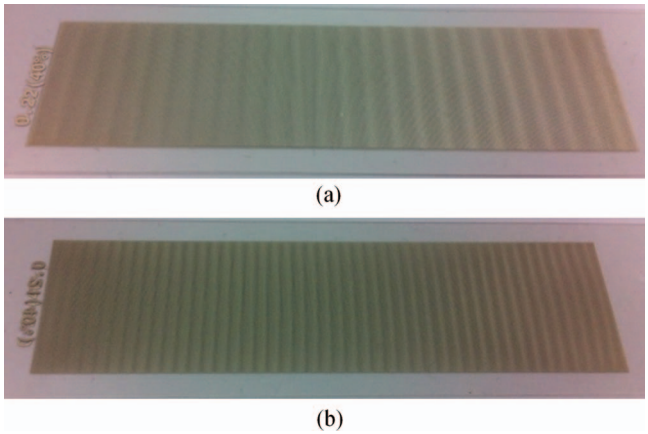

FIG. 4. Moiré patterns: (a) Moiré pattern with the pitches of 0.21 mm and 0.22 mm; (b) Moiré pattern with the pitches of 0.21 mm and 0.23 mm.

preferred for the image sensor. In the proposed algorithm, the pitch of the printed scale grating is estimated by Eq. (1). Because the pitch of the reticle grating is precisely manufactured by the photo-lithographic process and is known, the pitch of the scale grating can be estimated using Eq. (1) if the pitch of the envelop of the moiré image can be measured accurately. To measure the envelop frequency, the Fast Fourier Transform (FFT) method is used. To improve the frequency resolution of the FFT method, a longer image sensor is preferred.

A flow chart of the proposed algorithm is presented in Fig. 5. The flow chart shows one cycle of signal processing for each time stamp, and this is repeated for every sampling period of the image sensor. In the first step, the light intensity data array of 1024 pixels is gathered on the NMOS image sensor, as shown in Fig. 6(a). Because we are interested in only the envelop frequency of the moiré image in Eq. (1), the array is filtered in low pass by an MA filter and the filtered signal is given in Fig. 6(b). Before carrying out FFT on this signal, the Gaussian window is applied to this signal as shown in Fig. 6(c) to improve the accuracy of frequency peak detection using parabolic interpolation.[14] When applying the Gaussian window, the spectral peak maximum located between two discrete spectrum bins becomes parabola in the logarithmic scale, and accurate peak detection will be enabled by parabolic interpolation. The signals from Fig. 6(c) are transformed from the spatial domain into the spatial frequency domain by the FFT method, and the lower spectral peak is interpolated by parabolic fitting using three bins near the maximum point. Figure 7 shows this procedure. The pitch of scale can be calculated by the following equation, which is a modified version of Eq. (1):

$$P_s = P_r P_b/(P_b - P_r), \tag{6}$$

where P_r is the pitch of reticle grating and P_b is the pitch of the envelop of moiré image. The accuracy of the pitch estimation algorithm is confirmed by a simulation based on the configuration of the proposed system. If the pitch and linewidth of the reticle grating and the scale grating are given, the raw signal of the image sensor can be generated by a simulation. By comparing the given pitch of the scale grating and the estimated pitch from the algorithm, the estimation accuracy of the algorithm can be evaluated. To observe the effect of scale movement in a real situation, the raw signal of the image sensor is repeatedly generated at a sampling rate of 2 kHz while the scale grating is moving at 100 mm/s relative to the other components. The result of the comparison is given in Fig. 8, and the estimation error is less than 10 nm.

To obtain a set of phase-shifted signals ($I_{0,i}$, $I_{90,i}$, $I_{180,i}$, and $I_{270,i}$), the image sensor is structured as shown in Fig. 9. Each region of the phase-shifted signal is determined by a quarter of the pitch of the envelop in the moiré pattern. Several pixels belong to each phase-shifted signal, and subscript (i) means the index of each set of phase-shifted signals because a set of phase-shifted signals is repeated in the image sensor.

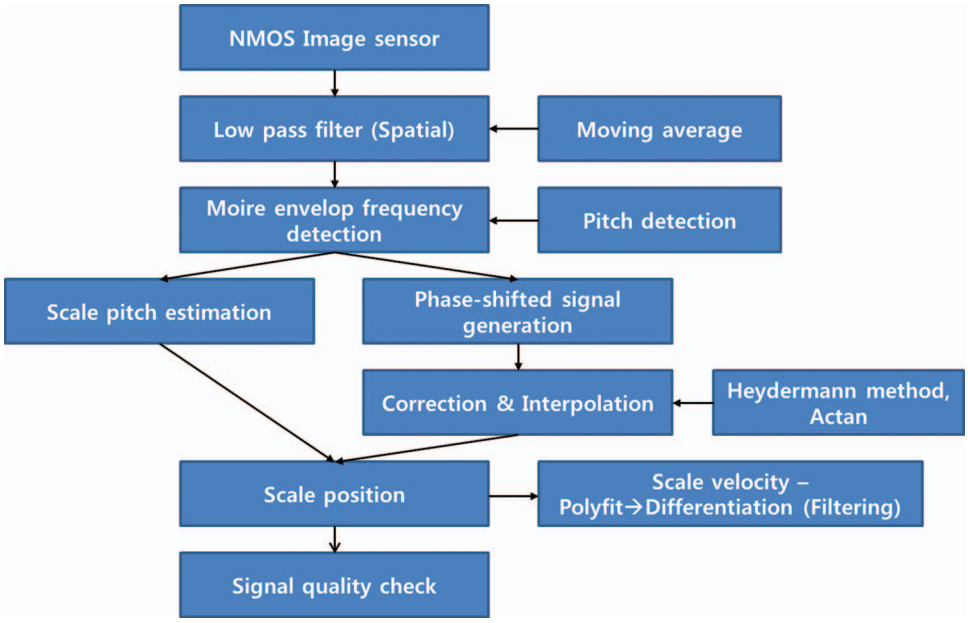

FIG. 5. Flow chart of the proposed printed grating scale encoder.

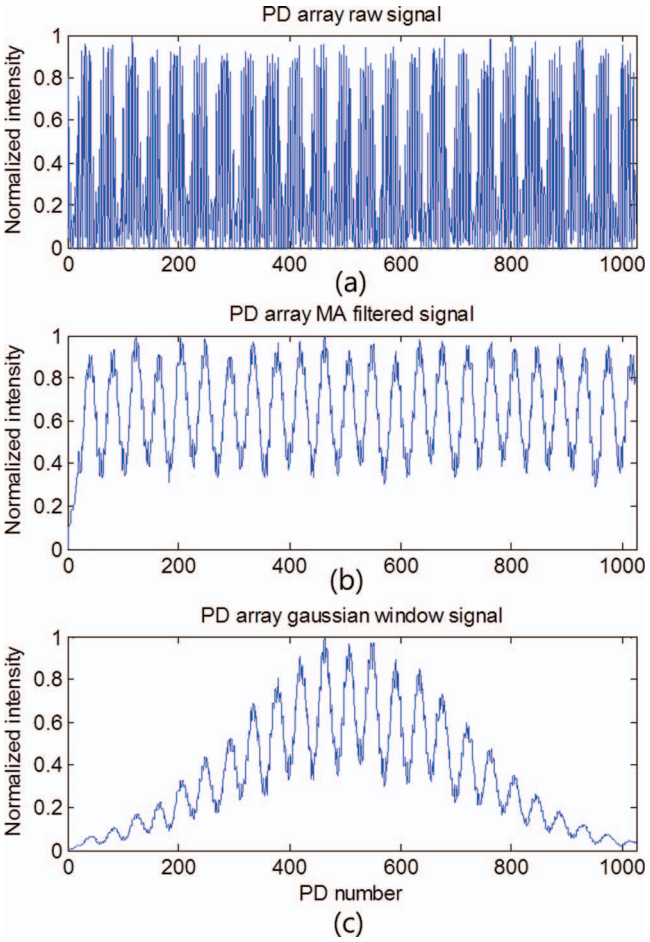

FIG. 6. Signal processing procedure of image sensor data to estimate the pitch of the printed scale grating: (a) raw data from image sensor; (b) MA-filtered signal of raw data; (c) Gaussian window applied to MA filtered signal.

Finally, four phase-shifted signals (I_0, I_{90}, I_{180}, and I_{270}) are acquired by averaging all the pixels that belong to the relevant phase signal. For example, I_0 can be obtained by averaging all the pixels that belong to $I_{0,i}$. The points of the Lissajous

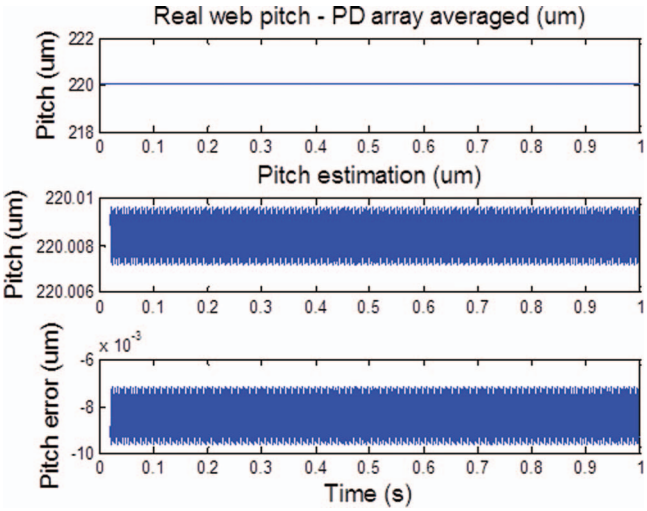

FIG. 8. Evaluation of the pitch estimation algorithm based on the simulation.

curve are generated by two signals (I_1, I_2) like in a traditional encoder. In measuring displacement with the encoder, only the difference in position between two adjacent time stamps can be measured by means of the phase difference between two time stamps. In other words, the phases at more than two time stamps should be calculated using the same pitch. In this step, it is assumed that the difference in real pitch between two time stamps is negligible because the measurement time difference and the measured position difference on the scale grating are negligible. Under this assumption, the k-1th and kth time stamps will be handled with the pitch of the kth time stamp. The phase difference between the two time stamps is calculated as shown in Fig. 10, and the equation is given in Eq. (7) as follows:

$$\theta^k = \arctan 2\left(I^k_{1,k}/I^k_{2,k}\right) - \arctan 2\left(I^k_{1,k-1}/I^k_{2,k-1}\right), \qquad (7)$$

where θ is the calculated phase difference, the superscript is the time stamp at calculation, and the subscript is the time stamp upon gathering the image data. The repeated cycle of

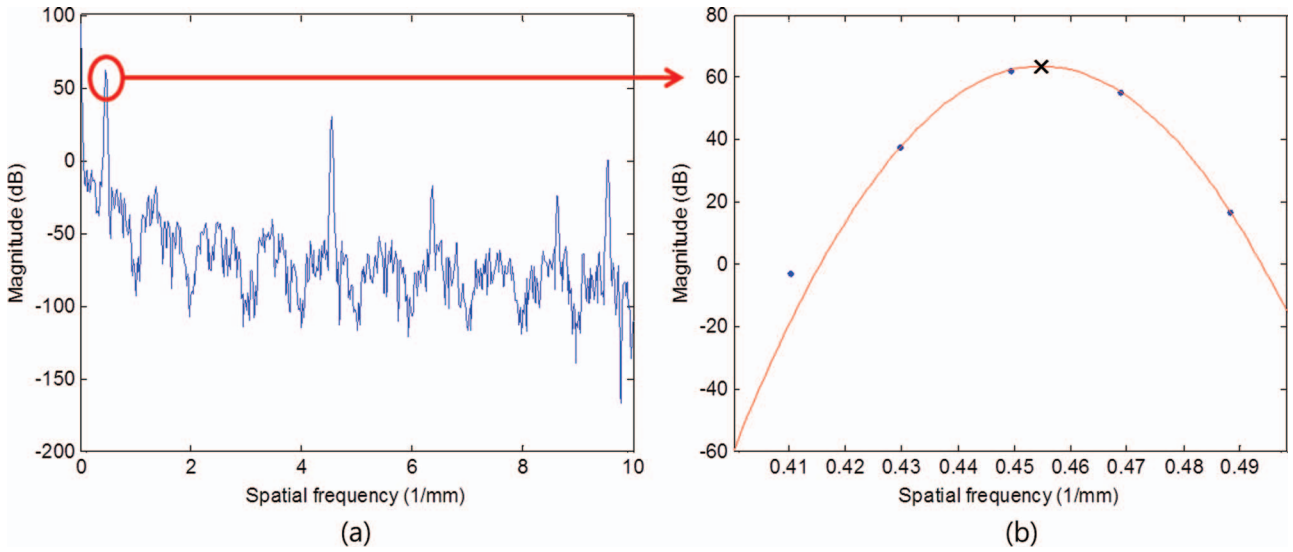

FIG. 7. Signals in spatial frequency domain: (a) FFT result of MA-filtered signal with Gaussian window in logarithm scale; (b) spectral peak detection by parabolic interpolation.

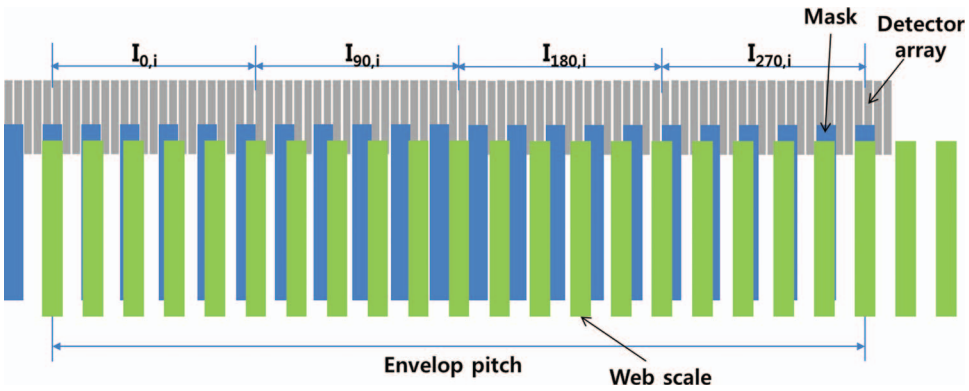

FIG. 9. Structured image sensor to obtain the phase-shifted signal.

the algorithm generates the successive θ^k. The final displacement is calculated by Eq. (4).

The above algorithm is evaluated with constant pitch and constant line-width, and the results are presented in Fig. 11(a). When assuming that the scale web is moving at constant speed, the position error of the propopsed method is simulated and the error increases with the displacement of the web scale. The main reason for this is the distortion of the Lissajous curve with respect to a unit cricle in the printed web scale encoder. Actually, the amplitude difference of I_1 and I_2 is a major contribution as shown in Fig. 11(b). The mean, phase offset and amplitude difference in the Lissajous circle can be corrected by the Heydermann method.[14] However, two points in the Lissajous curve are not enough to apply the Heydermann method, and data points which can show a complete Lissujous circle are required. The modified algorithm, for which more time stamps are averaged, is shown in Fig. 12. The required number of time stamps is determined by the sampling freqency and web movement velocity using Eq. (8). To improve the accuracy of correction, plenty of time stamps are used in this study, with the minimum number of averaged time stamps set at 20:

$$n = \begin{cases} 20, & if \ \dfrac{2\pi \cdot v}{P_s \cdot F_s} \geq \dfrac{\pi}{10} \\ \dfrac{P_s \cdot F_s}{v}, & if \ \dfrac{2\pi \cdot v}{P_s \cdot F_s} < \dfrac{\pi}{10} \end{cases}, \tag{8}$$

where n is the number of averaged time stamps and v is the velocity of the web. After applying the Heydermann correction, the Lissajous curve almost becomes a unit circle and the displacement error is clearly reduced, as shown in Fig. 11.

The velocity of the web is calculated by differentiation of the displacement. To reduce noise in differentiation, a time stamping method that uses polynomial fit using previous and present positions is applied.[15] In this paper, the first order fitting and five time stamps are used.

Finally, the generated sinusoidal signals should be qualified if it is well-conditioned to represent the web displacement or not. In cases where the printing quality is poor or an abrupt change of pitch in the scale grating occurs during handling of the web, each sinusoidal signal may become too distorted, thus resulting in a deterioration of measurement accuracy. The signal quality (SQ) is calculated by Eq. (9), which expresses the deviation of the Lissajous curve from the unit circle,

$$SQ = 1 - \sum_{i=1}^{n} \frac{d_i}{n}, \tag{9}$$

where d_i represents the distance of the ith point in the Lissajous curve from the unit circle.

III. PERFORMANCE EVALUATION BY SIMULATION

The proposed algorithm was simulated using Matlab (by Mathworks Inc.) to prove the validation of the algorithm under the variations of pitch and line-width in the printed scale grating. To determine the levels of variation in the simulation,

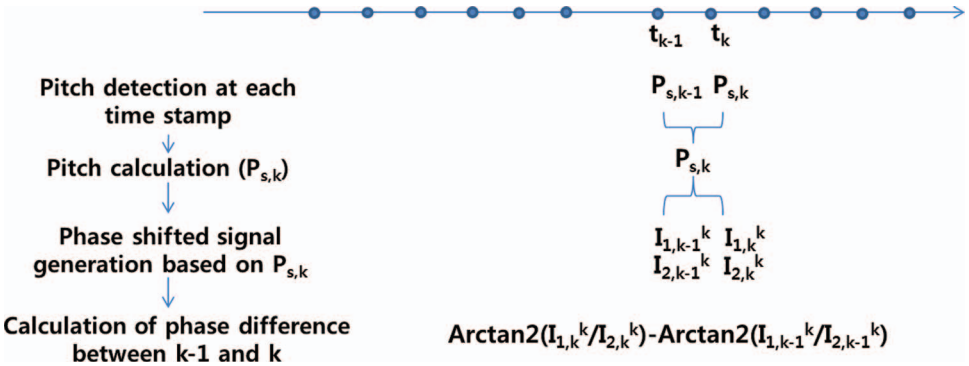

FIG. 10. Calculation of delta phase between two successive time stamps.

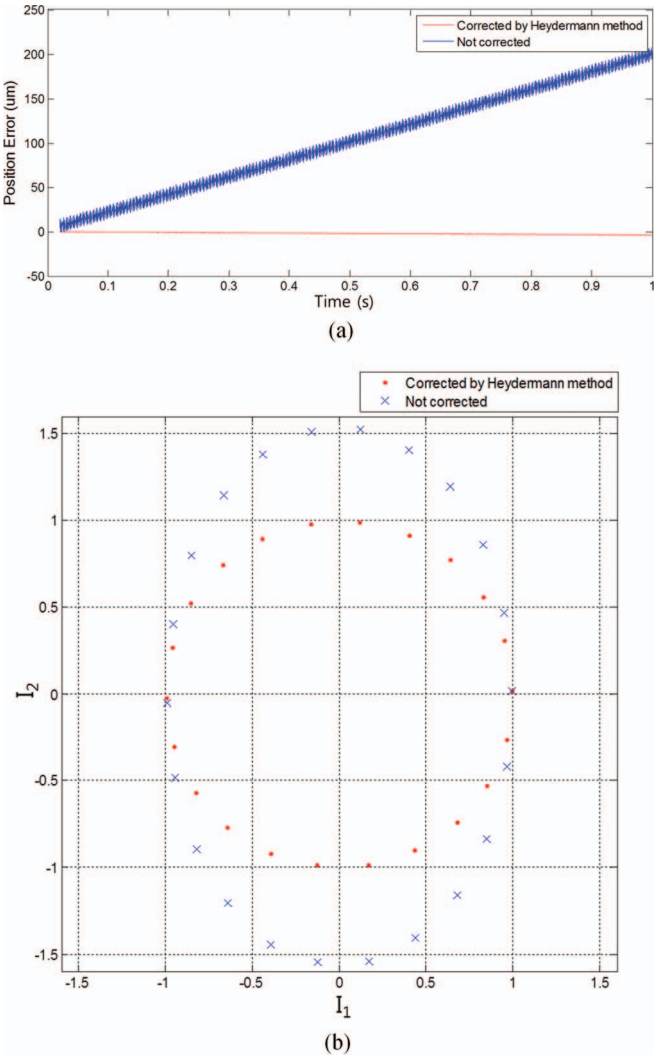

FIG. 11. Simulation of web movement at constant velocity using constant pitch and line-width with and without Heydermann correction method: (a) result of comparison of web displacement; (b) result of comparison of the Lissajous circle.

screen printed grating patterns were evaluated in advance. Six samples were prepared. Those pitches were 210 μm, 220 μm, and 230 μm, and the duty ratios of 40% and 60% were applied to each pitch sample. Each sample was measured using an optical microscope with a pixel resolution of 1.84 μm at three positions, as shown in Fig. 13(a). The measured image was averaged vertically and the pitch and line-width were determined by edge detection using the threshold of mean intensity. The pitches were calculated by the distance between two adjacent rising edges and the line-width was obtained by the distance from a falling edge to the nearest rising edge in the right direction. To determine the exact edge position, two pixels near the threshold were interpolated based on the intensity. This procedure is presented in Fig. 13(b). The average value and standard deviation of the pitch and line-width in each sample are plotted in Fig. 13(c). 1σ of the pitch variation was less than 2.2 μm and 1σ of the line-width variation was less than 6.0 μm.

In the first simulation, the effects of variations in pitch and line-width were evaluated by comparing the measurement error in cases where there were variations in pitch and line-width with the error when there were no variations in pitch and line-width. Most simulations in this section were done under the condition that the web is moving at a velocity of 100 mm/s (6 m/min) because the typical line speed for printed electronics is less than a few m/min. While line speed larger than 100 m/min can be used in media printing line, the lower speed is generally used in line for printed electronics because the printing quality and registration should be managed better in printed electronics than in media printing. The variations in pitch and line-width were randomly generated from the standard normal distribution. The mean pitch was set at 220 μm, 1σ of the pitch variation was 2.2 μm and 1σ of line-width variation was 5.5 μm. It was assumed that the scale was moving at a constant velocity of 100 mm/s, and the measurement errors are shown in Fig. 14. When there are no variations in pitch and line-width, the error linearly increases up to about

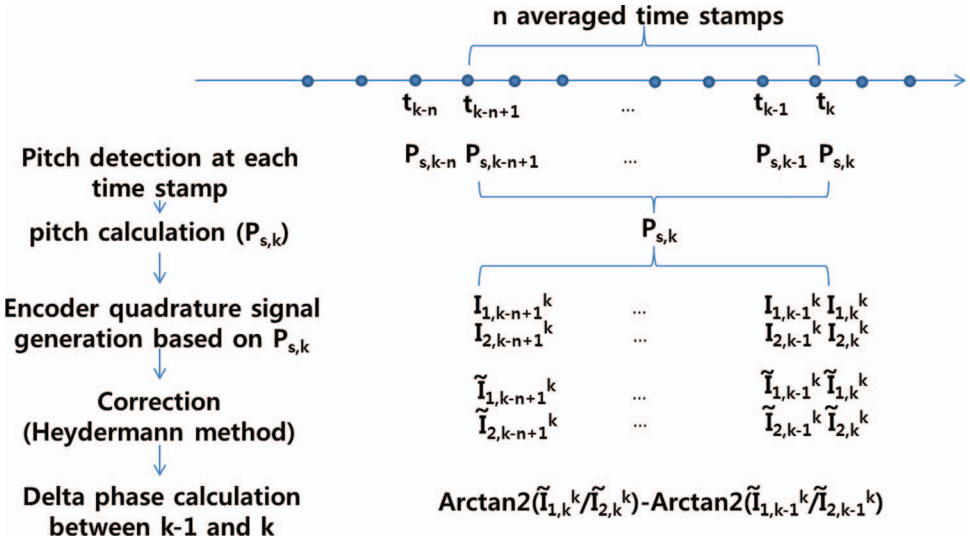

FIG. 12. The modified algorithm for which more time stamps are averaged and Heydermann method is applied to correct the Lissajous curve into a unit circle.

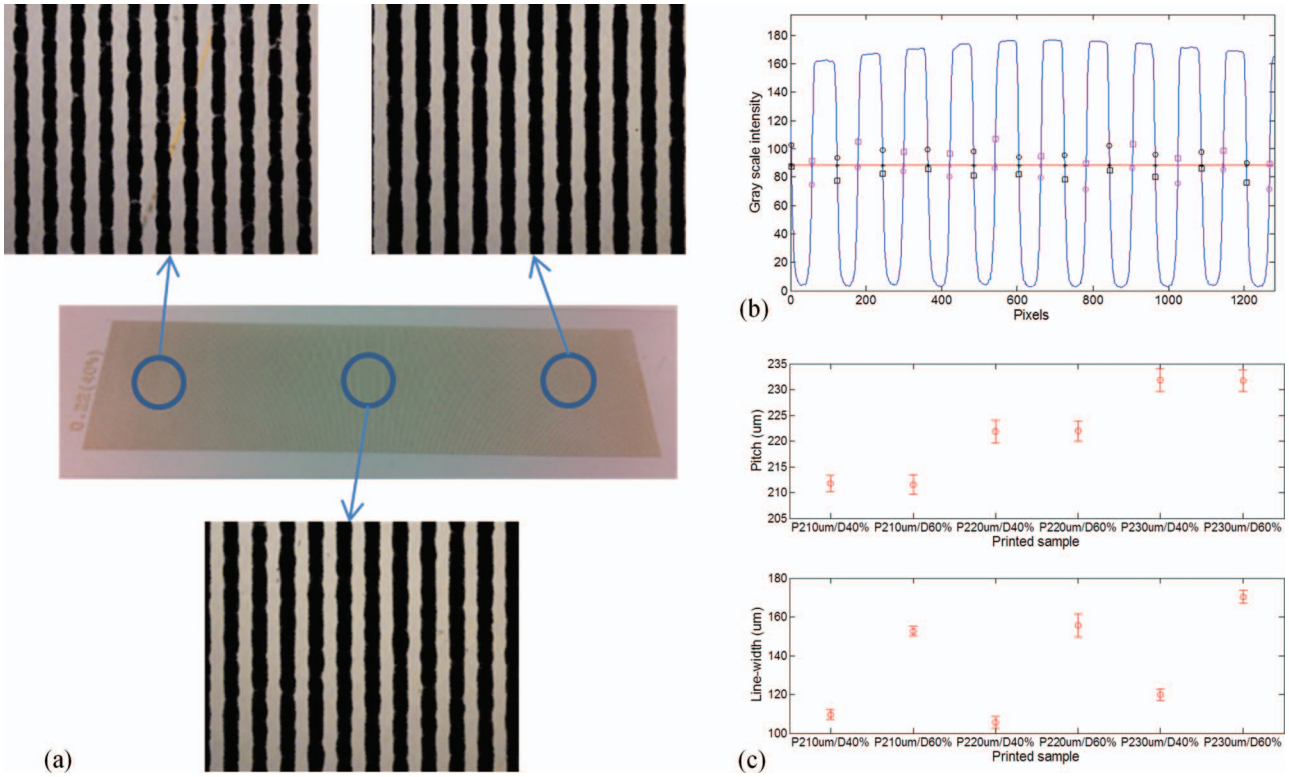

FIG. 13. Measurement of variations in pitch and line-width in screen printed gratings: (a) measurement method; (b) example of determining pitch and line-width in each optically measured pattern image; (c) Average value and standard deviation of the pitch and line-width in each sample.

4 μm over a travel distance of 100 mm, as shown in Fig. 14(a). This linearly increased error is related to the accuracy of pitch estimation as shown in Fig. 8. The accuracy of pitch estimation is proved by about 8 nm when the pitch of the scale grating is 220 μm. This means that an error of about 40 ppm is inevitable, and results in a linearly increased displacement error of 4 μm for a movement of 100 mm. Figure 14(b) shows the error with line-width variation, and there is a slight impact on the measurement of displacement and velocity. However, the SQ decreases because variations in line-width cause a

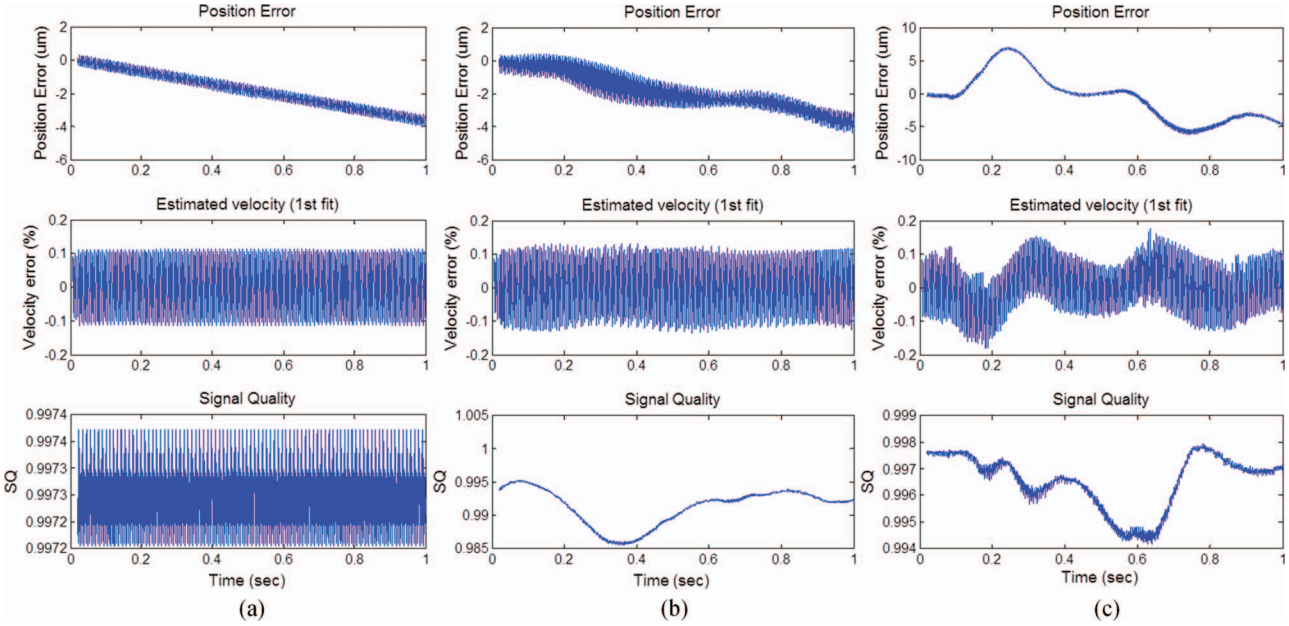

FIG. 14. Effect of variation in pitch and line-width on the measurement accuracy of displacement and velocity and signal quality: (a) no variation; (b) line-width variation; (c) pitch variation.

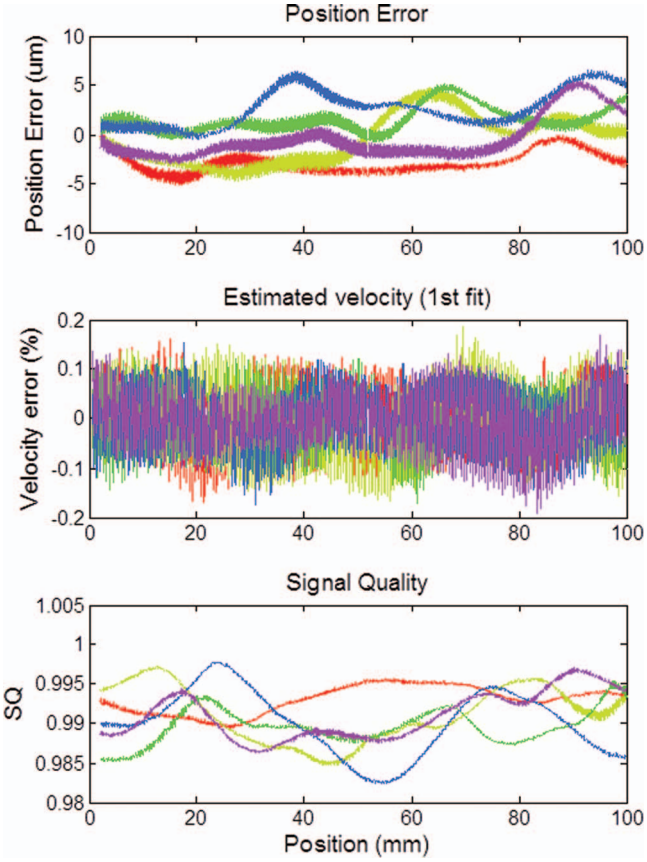

FIG. 15. Simulation of dependency on generated random variation in pitch and line-width.

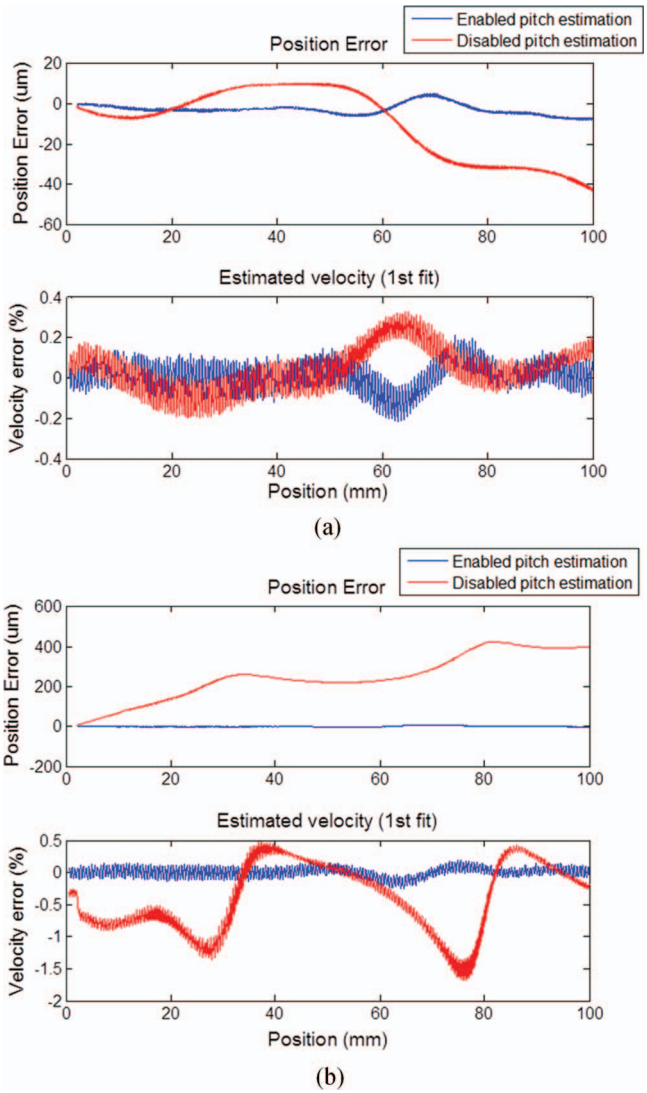

FIG. 16. Effectiveness of the pitch estimation algorithm on the measurement error: (a) without mean pitch offset error; (b) with mean pitch offset error of 1 μm.

distortion of the Lissajous circle. The effect of pitch variation is a bit dominant, as shown in Fig. 14(c). The displacement error increases up to 7.0 μm and the maximum velocity error to 0.2%. Five cases are additionally simulated in Fig. 15 to prove the feasibility of the algorithm for other variations in pitch and line-width, and all cases show similar results with Fig. 14(c). In this simulation, variations in both line-width and pitch are included at the same time.

Second, the effectiveness of the pitch estimation algorithm was evaluated, pitch and line-width were randomly varied, and the measurement error without the pitch estimation algorithm was compared with the error using the pitch estimation. In cases where there was no pitch estimation, it was assumed that the pitch was printed in the same form as the plate master, with the pitch of the plate master being 220 μm. In Fig. 16(a), the pitch variation is generated with a mean of 220 μm and a standard deviation of 2.2 μm, and the line-width variation is generated by a mean of 110 μm and a standard deviation of 6 μm. The error increases from 8.3 μm to 43.5 μm without using the pitch estimation. Figure 16(b) shows the simulation results of the case where the printed grating has a mean pitch offset of 1 μm from the plate master. The mean pitch changes from 220 μm to 221 μm while the other variation remains the same as in Fig. 16(a). Due to the offset of mean pitch, the displacement error increases to 421 μm and the maximum velocity error increases to 1.7%. Because the mean offset error in the printed scale grating may easily be caused by a misaligned angle between the scale grating and the image sensor, the pitch estimation becomes more important.

The effect of the Heydermann correction method on measurement accuracy is presented in Fig. 11. Due to distortion of the Lissajous curve, the displacement error is linearly increased and the measurement noise within a pitch of the scale grating is enlarged. Figure 17 shows the correction trend of the DC offset of I_1, the DC offset of I_2, the phase shift between I_1 and I_2, and the amplitude ratio between I_1 and I_2 by the Heydermann method.

IV. EXPERIMENTS

The proposed algorithm was evaluated experimentally as presented in Fig. 18. The test setup was designed to prove the concept of the algorithm and compactness of system is not considered. The collimated beam was generated by a diode laser (#31-2772-000, Coherent Inc.) and a condenser lens, and

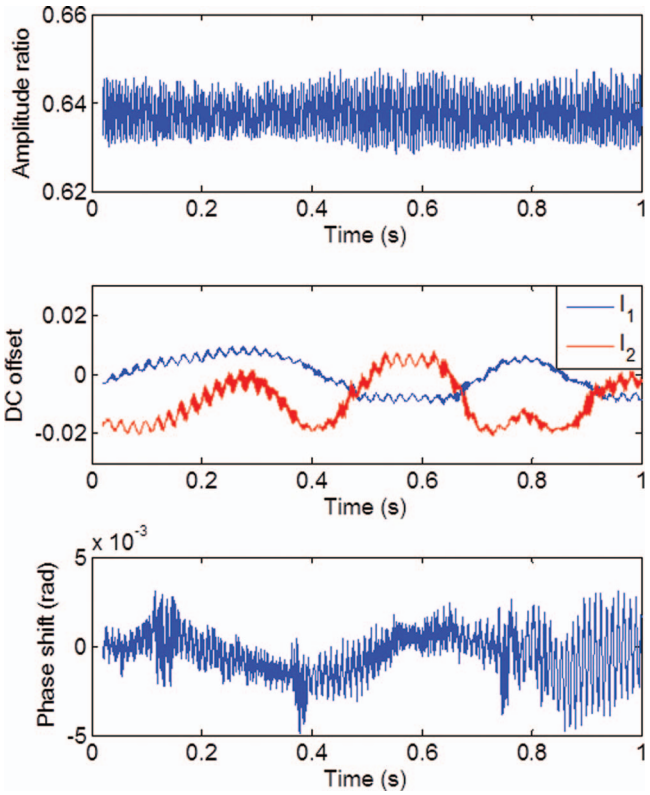

FIG. 17. Results of simulation of the correction parameter variation when applying the Heydermann correction method.

was projected on the reticle (Ronchi Rullings, 5.0 c/mm, Applied Images Inc.). A screen-printed grating with pitches of 210 μm, 220 μm, and 230 μm was used as the scale grating, and the transmitted moiré image was captured by the NMOS image sensor (S3901-1024Q, Hamamatsu Photonics K. K.). The movement of the printed scale grating was obtained by a LM guided linear motor stage. The image sensor data were gathered by an AD (Analog-to-Digital) data acquisition board (USB-6366, National Instrument Corp.), and the signal processing was done by Matlab in off-line because it is out of scope in this paper to develop the real-time signal processing board even though the signal processing should be done in real time. Due to the sampling rate of the AD board, the test was carried at a velocity of 10 mm/s. Displacement and velocity were compared with the linear encoder (MS80.00-2G, RSF Electronik G.m.b.H.), which was implemented in the linear motor stage to verify the accuracy of the proposed encoder. Because time for data acquisition and signal processing is in closely connected with the maximum operation speed of the encoder, high-speed data acquisition and signal processing will be next research target for the practical implementation and commercialization of the proposed encoder.

Before the test, the alignment angle between the reticle grating and the image sensor was calibrated. When the reticle grating and the image sensor were aligned in parallel, the pitch of the reticle grating could be treated by 200 μm. If not, the pitch of the reticle grating had to be calibrated by the following equation:

$$P_{r,c} = (1 - \cos\theta_m)P_r \tag{10}$$

where P_r is the pitch of the reticle grating, $P_{r,c}$ is the corrected pitch of the reticle grating, and θ_m is the misaligned angle between the reticle scale and the image sensor. The same method (as the previously explained pitch estimation of the moiré image) was used to correct the pitch of the reticle grating. The light projected through the reticle grating without the scale grating was captured at the image sensor and the spectral peak was detected by parabolic interpolation in the logarithmic scale. The corrected pitch of the reticle grating was 199.369 μm in the test setup.

The test results are presented in Fig. 19. Figure 19(a) shows the results when the used pitch of the scale grating was 210 μm and the duty ratio of the line-width was 40%. A similar test was performed with pitches of 220 μm and

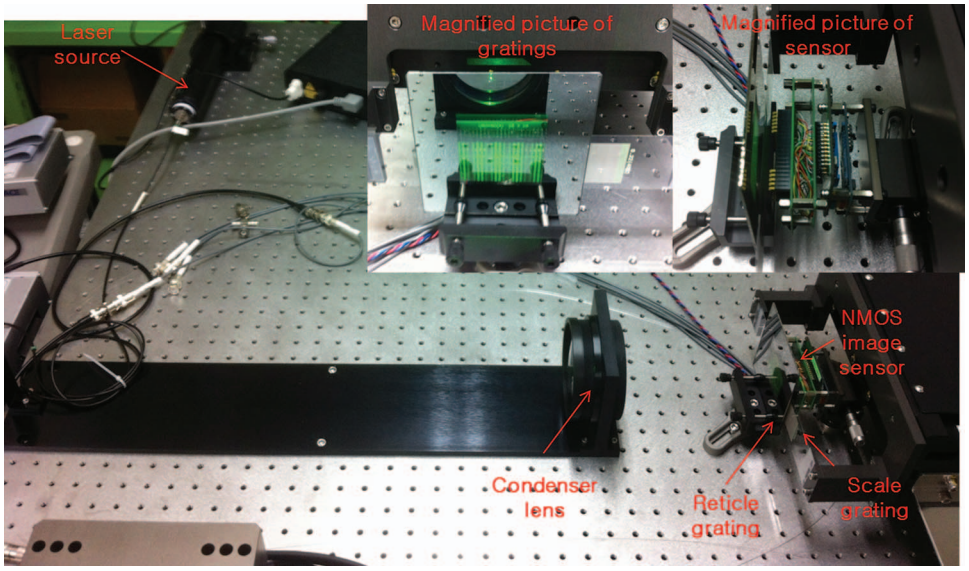

FIG. 18. Experimental setup to evaluate the proposed algorithm.

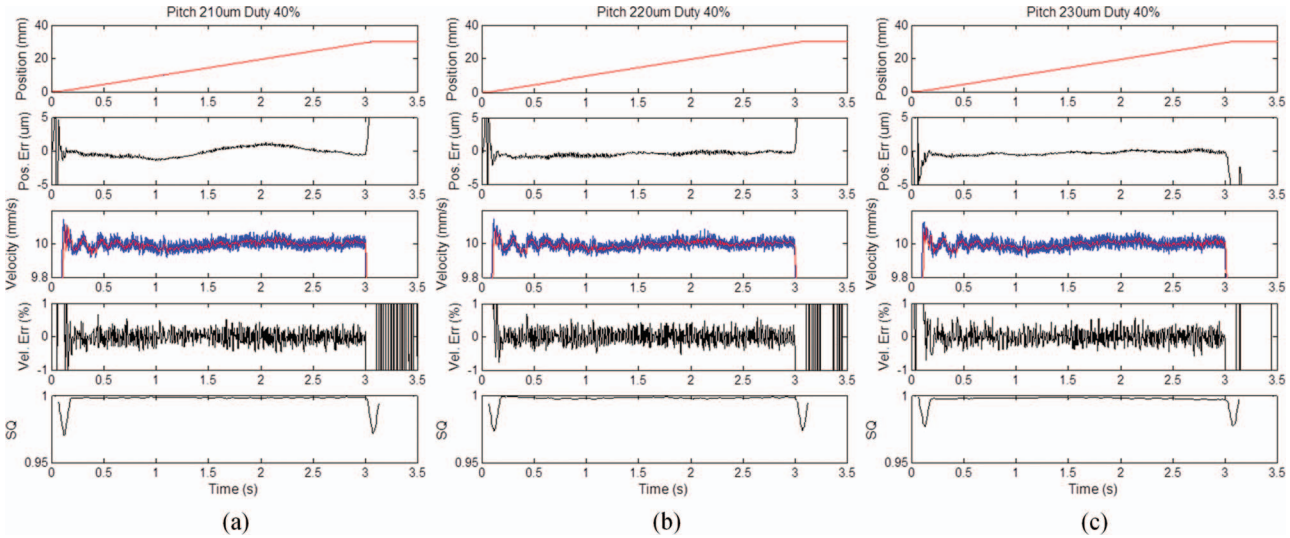

FIG. 19. The measurement error according to different grating pitches: (a) pitch of 210 μm; (b) pitch of 220 μm; (c) pitch of 230 μm.

230 μm, the results of which are shown in Figs. 19(b) and 19(c). The displacement error was less than 2.5 μm and the velocity error of 1σ was about 0.25%, while the grating scale moved 30 mm. In Fig. 19, the most ripples in velocity were caused by the high frequency component of the linear encoder. The capability to capture the high frequency component was evaluated by splitting the number of data points for the time stamping method of calculating velocity. The blue line in Fig. 20 shows that the differentiation noise of the proposed encoder limits improvement of accuracy when measuring velocity because the error is increased by reducing the number of data points, and five data points are actually optimal for estimating velocity. The red line in Fig. 20 shows the velocity error when the time stamping method is applied to both the printed web scale encoder and the linear encoder. In this case, the 1σ error is well reduced to about 0.05% and the low-frequency component is measured accurately.

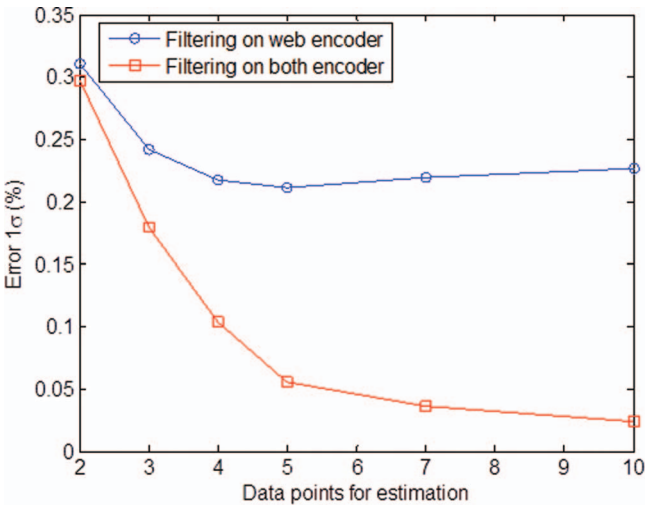

FIG. 20. Velocity measurement error of 1σ according to the number of data points used in the time stamping method for the velocity estimation.

V. CONCLUSION

A novel algorithm for measuring the movement of the flexible web in a roll-to-roll manufacturing systems with a printing process is proposed. The developed algorithm is based on the traditional single field encoder principle, and the scale grating is replaced with a printed grating on the web. Because the printed grating cannot be as accurate as the scale grating in the traditional encoder, there will inevitably be variations in pitch and line-width. The developed method of measurement can measure the motion of the web precisely even though there are variations in pitch in the printed grating patterns. For this reason, the developed algorithm includes a method of estimating the variations in pitch precisely. In addition, a method of correcting the Lissajous curve to a unit circle based on the Heydermann method is proposed to improve the phase interpolation accuracy. The performance of the developed method is evaluated by simulation and experiment. In the experiment, the displacement error is less than 2.5 μm and the velocity error of 1σ is about 0.25%, while the grating scale moves 30 mm.

ACKNOWLEDGMENTS

This work was partially supported by both the government-funded research program of the Korea Research Council for Industrial Science and Technology (ISTK) and the Industrial Strategic Technology Development Program (10041041) funded by the Ministry of Knowledge Economy (MKE, Korea).

[1]H. J. Levinson, *Principle of Lithography* (SPIE Press, 2005).
[2]Minhoon Jung, Jaeyoung Kim, Jinsoo Noh, Namsoo Lim, Chaemin Lim, Gwangyong Lee, Junseok Kim, Hwiwon Kang, Kyounghwan Jung, Ashley D. Leonard, James M. Tour, and Gyoujin Cho, IEEE Trans. Electron Devices **57**, 571 (2010).
[3]Frederik C. Krebs, Org. Electron. **10**, 761 (2009).
[4]M. Bartzsch, U. Fuegmann, T. Fischer, U. Hahn, H. Pereissler, G. Schmidt, and A. Huebler, *NIP & Digital Fabrication Conference*, Digital Fabrication 2006 Final Program and Proceedings, pp. 13–16(4).

[5]Kee-Hyun Shin, Jeung-In Jang, Hyun-Kyoo Kang, and Seung-Ho Song, IEEE Trans. Ind. Appl. **39**, 1422 (2003).
[6]Kyung-Hyun Choi, Thanh T. Tran, and Dong-soo Kim, J. Adv. Mech. Des. Syst. **5**, 7 (2011).
[7]Kee-Hyun Shin and Soon-Oh Kwon, IEEE Trans. Ind. Appl. **43**, 403 (2007).
[8]Chung Hwan Kim, Ha-Il You, and Seung-Hyun Lee, Proc. Inst. Mech. Eng., Part C: J. Mech. Eng. Sci. **226**, 2726 (2012).
[9]Yongsoon Eun, Jeffrey J. Folkins, and Jess R. Gentner, U.S. patent 8,346,503 B2 (2013).
[10]Barclay J. Tullis, U.S. patent 6,118,132 (2000).
[11]Dongho Oh, KR patent application 10-2010-0075319 (2010) (Korean).
[12]K. K. Tan, H. X. Zhou, and Tong Heng Lee, IEEE. Trans. Instrum. Meas. **51**, 1073 (2002).
[13]See www.heidenhain.com.
[14]M. Gasior and J. L. Gonzalez, AIP Conf. Proc. **732**, 276–285 (2004).
[15]R. J. E. Merry, M. J. G. van de Molengraft, and M. Steinbuch, Mechtronics **20**, 20 (2010).